Role of Carrier Transport in Source and Drain Electrodes of High-Mobility MOSFETs

Tsuchiya, Hideaki
Maenaka, Akihiro
Mori, Takashi
Azuma,Yusuke

(Citation)
IEEE Electron Device Letters,31(4):365-367

(Issue Date)
2010-04

(Resource Type)
journal article

(Version)
Accepted Manuscript

(URL)
https://hdl.handle.net/20.500.14094/90001272

Role of Carrier Transport in Source and Drain Electrodes of High-Mobility MOSFETs

Hideaki Tsuchiya, *Senior Member*, *IEEE*, Akihiro Maenaka, Takashi Mori, and Yūsuke Azuma

***Abstract*—We have studied the performance potentials of III-V semiconductors and Ge *n*-channel MOSFETs based on a quantum-corrected Monte Carlo device simulation. We found that as a ballistic limit is approached, III-V MOSFETs lose their inherent advantage over Si and Ge MOSFETs because current enhancement due to ballistic transport becomes less effective than in Si and Ge channels. However, a high source and drain doping concentration was found to greatly improve the performance of III-V MOSFETs by reducing parasitic resistance and the mitigation of 'source starvation' attributed to the low density-of-states.**

***Index Terms*—High mobility MOSFETs, ballistic transport, parasitic resistance, source starvation, Monte Carlo simulation**

I. Introduction

The remarkable advancement of LSI circuit technology has been primarily based on the downsizing of MOSFETs. However, in the present post-scaling era, downsizing has become less effective because conventional Si CMOS scaling has been reaching its fundamental limits. As a new challenge, the application of high mobility materials such as III-V semiconductors and Ge to MOSFET channels is expected to achieve better device performance without miniaturization [1].

To clarify the advantages of introducing high mobility materials into MOSFET channels, we have developed a quantum-corrected Monte Carlo device simulator (MONAQO) that considers the material bandstructure, scattering processes and quantization in the inversion layer [2,3]. Using MONAQO, we have demonstrated that the introduction of an ultrathin-body (UTB) structure is indispensable for minimizing short channel effects and enhancing the current drive in III-V MOSFETs, since the electron wave-functions spread deeply into the substrate region due to the small quantization mass [2]. Thus, we employ a UTB structure in this paper and evaluate the on-current properties of high mobility MOSFETs based on MONAQO, taking particular interest in a comparison with Si MOSFETs. We demonstrate that a high source and drain (S/D) doping concentration is needed for III-V MOSFETs to outperform Si and Ge MOSFETs definitely, which is crucial particularly in the quasi-ballistic regime.

Manuscript received July, 2009.

The authors are with the Department of Electrical and Electronics Engineering, Graduate School of Engineering, Kobe University, 1-1, Rokko-dai, Nada-ku, Kobe 657-8501, Japan (e-mail: tsuchiya@eedept.kobe-u.ac.jp).

II. Simulation Model

Table 1 shows the band parameters used in the simulation. It is well known that in III-V materials and Ge, electron transfer to the higher valleys with a heavier transport mass degrades the device performance significantly [1]. Therefore, the energy differences between the lowest and higher valleys ($\Delta E_{\Gamma L}$, $\Delta E_{L\Gamma}$ and ΔE_{LX}) are important physical parameters. Note also that the nonparabolicity of the Γ valley is the largest for $In_{0.53}Ga_{0.47}As$, which may be disadvantageous for rendering a higher carrier velocity. The device structure is shown in Fig. 1, where we employ a UTB structure with a Si-layer thickness of 5 nm. A Ge (111) surface orientation [1,2,3] and strained-Si channels under 1% biaxial and uniaxial tensile strains are also considered. The band-edge energy variation due to the biaxial (uniaxial) strain was given by ΔE_{2f} = -0.25eV (-0.125eV) and ΔE_{4f} = -0.04eV (-0.016eV) for the 2-fold and 4-fold valleys, respectively [4]. The effective mass variation due to the uniaxial tensile strain was taken into account based on a first-principles bandstructure calculation [5]. We considered impurity and phonon scatterings in the simulation [2,3], while roughness and electron–electron scatterings are ignored to evaluate the intrinsic device performance of each material. For impurity scattering, we considered Fermi–Dirac statistics to calculate the screening length, which is particularly important for III-V materials [6]. The electrical characteristics were simulated by MONAQO [2,3,7], which incorporates a quantum correction of the potential represented in the form of a density-gradient, the validity of which has been demonstrated by a comparison with the Schrödinger–Poisson solution for inversion-layer electrons [7].

		Si	Ge	GaAs	InP	$In_{0.53}Ga_{0.47}As$
mobility ($cm^2V^{-1}s^{-1}$)		1600	3900	9200	5400	25000
mass (Γ)		–	0.037	0.063	0.082	0.046
mass (X)	m_t (m_0)	0.19	0.29	–	–	–
	m_l (m_0)	0.98	1.35	–	–	–
mass (L)	m_t (m_0)	–	0.082	0.127	0.153	0.125
	m_l (m_0)	–	1.59	1.538	1.878	1.552
nonparabolicity α		0.5 (X)	0.65 (L, Γ, X)	1.16 (Γ) 0.40 (L)	0.61 (Γ) 0.49 (L)	1.18 (Γ) 0.43 (L)
$\Delta E_{\Gamma L}$ (eV)		–	–	0.323	0.832	0.723
$\Delta E_{L\Gamma}$ / ΔE_{LX} (eV)		–	0.14 / 0.18	–	–	–
permittivity ε_r		11.9	16.0	12.9	12.6	14.1
E_f of S/D (eV)		0.064	0.131	0.274	0.326	0.576

Table 1. Parameters used in the simulation. Fermi energies (E_f) corresponding to the S/D donor concentrations N_D = 1×10^{20} cm^{-3} for Si and Ge and N_D = 2×10^{19} cm^{-3} for III-V materials are also indicated.

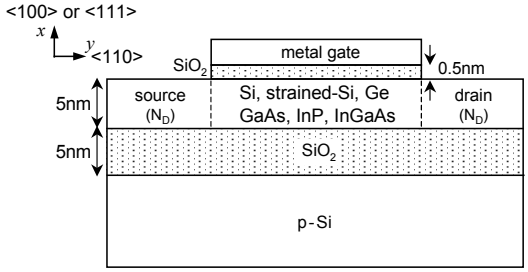

Fig. 1. Device model used in the simulation, where a UTB structure and intrinsic channel are employed.

The solid solubility of donors in III-V semiconductors is limited to less than or comparable to 2×10^{19} cm^{-3} [8]. So, we assigned $N_D = 2\times10^{19}$ cm^{-3} for III-V materials and a higher value of $N_D = 1\times10^{20}$ cm^{-3} for Si and Ge. While implant-free devices are of current interest, implanted devices including regrown source are also subject to active research [6,9,10]. We further point out that the Fermi energies of high mobility materials are much higher than that of Si [8], comparable to $\Delta E_{\Gamma L}$ and ΔE_{LX}. Therefore, a certain number of electrons already populate the higher valleys inside the S/D region and affect the device performance under ballistic transport [3].

III. Current Drive of III-V UTB MOSFETs

Figure 2 shows the channel length dependences of the on-current for all channel materials computed at (a) V_G-V_{th} = 0.3 V and (b) 0.7 V. The drain voltage V_D is set sufficiently small (0.5 V), thus band-to-band tunneling considered in [11] was ignored in this study. In Fig. 2(b), the GaAs channel degrades due to the Gunn effect. In the figures, ballistic-limit data for each material are also plotted as B. L., which were obtained by Monte Carlo simulations ignoring any scattering processes in the channel region. This gives the ideal device performance of the MOSFET, which has been shown to yield an equivalent result to Natori's model [12]. Although some revisions may be needed for nanoscale devices [6], we use here the above qualitative guideline to understand the ballistic limit. First, as Fischetti and Laux pointed out for sub-0.1-μm devices [8], the current drive of a device appears to be largely independent of the material, with the exception of In-based materials, even for the channel lengths of several tens of nanometers. However, it should be noted that the advantage of In-based materials decreases as the ballistic limit approaches, because ballistic transport is more effective in group IV materials. In other words, III-V MOSFETs are already quasi-ballistic in the present channel lengths. Incidentally, the calculated current drive in Fig. 2 is higher than that of the corresponding experimental results, because roughness scattering is ignored in the present calculation.

To understand such a limited performance enhancement in III-V MOSFETs, we discuss the role of carrier transport in the source and drain electrodes. First, to recognize the influence of the lower S/D donor concentration in III-V MOSFETs, we plot potential energy profiles in Fig. 3 for (a) Si, (b) biaxial strained-Si, (c) Ge (111) and (d) InP channels, where the results for each valley are also plotted. As shown by the solid lines in Fig. 3(d), a large potential drop appears in the drain region of the InP-MOSFET, which represents significant parasitic resistance owing to the lower donor concentration and intensified optical phonon scattering in the drain region. As a result, the channel electrical field decreases.

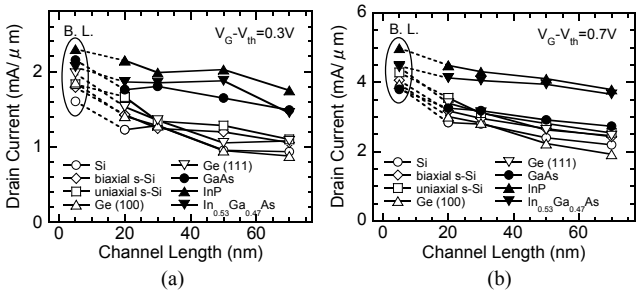

Fig. 2. Channel length dependences of on-current for all channel materials, where (a) V_G-V_{th} = 0.3 V and (b) 0.7 V. V_D = 0.5 V. B. L. represents ballistic-limit data. The degradation of the GaAs channel in (b) is due to the Gunn effect.

We next increased the S/D donor concentration in the III-V MOSFETs up to $N_D = 1\times10^{20}$ cm^{-3}, as a trial. Such a high donor concentration has been reported to be possible for InP using Te-doping [13] and Si-doping [14]. The potential profiles for such heavily-doped S/D are also plotted in Fig. 3(d) by the dashed lines. Although the potential barrier height at the source junction increases due to the increased Fermi energy of the source, the parasitic resistance is found to be ideally reduced by heavy doping. Further, Fig. 4 compares (a) averaged electron velocity and (b) sheet electron density between the lightly doped ($N_D = 2\times10^{19}$ cm^{-3}) and heavily doped S/D ($N_D = 1\times10^{20}$ cm^{-3}). Unexpectedly, the averaged velocity inside the channel is almost unchanged, as shown in Fig. 4(a). This is due to the

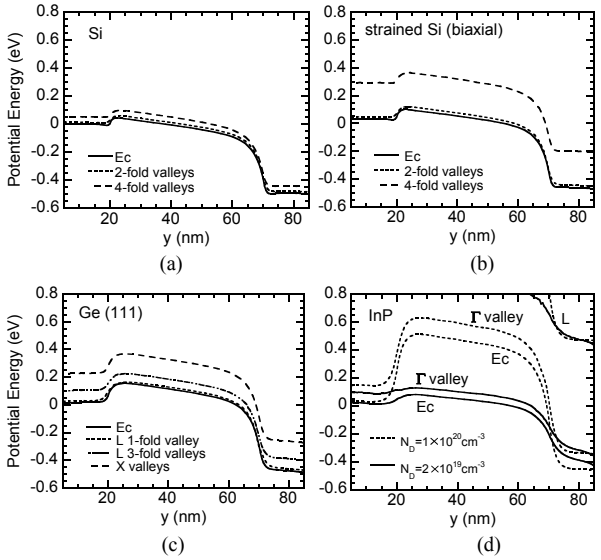

Fig. 3. Potential energy profiles for each valley in (a) Si, (b) biaxial strained-Si, (c) Ge (111) and (d) InP channels at V_G-V_{th} = 0.3 V and V_D = 0.5 V, where L_{ch} = 50 nm. Note that the quantum correction of the potential is included for each valley and thus the lowest valley is located above the conduction band-edge E_c. In (d), the results for heavily-doped S/D are also plotted by dashed lines.

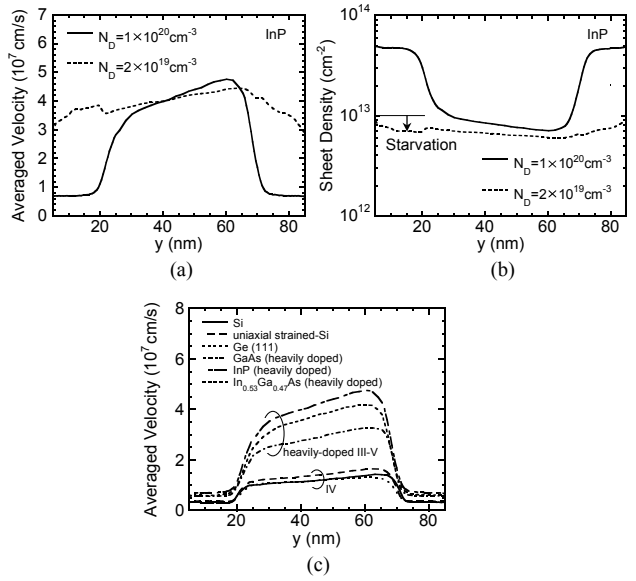

Fig. 4. Comparison of (a) averaged electron velocity and (b) sheet electron density profiles of InP-MOSFET between lightly-doped and heavily-doped S/Ds, where L_{ch} = 50 nm, V_G-V_{th} = 0.7 V and V_D = 0.5 V. 'Source starvation' appears in the lightly-doped source in (b). In (c), the averaged velocities are compared between various semiconductor channels.

fact that acceleration due to the enhanced channel field is offset by a reduction in the injection velocity from the source due to the increased impurity scattering. On the other hand, the sheet electron density inside the channel increases, as shown in Fig. 4(b). This is because the inability of the lightly-doped source to sustain a large flow of ballistic carriers heading into the channel, termed 'source starvation' [6,10], is avoided in the heavily-doped source which supplies more carriers that can be scattered due mainly to impurities and redistributed into the channel direction. In Fig. 4(c), we compare average electron velocities between Si, uniaxial strained-Si, Ge (111) and III-V MOSFETs, highlighting the high-speed capability of III-V MOSFETs, In-based materials in particular.

Due mainly to the lack of source starvation in heavily-doped S/D [6,10], the current drive of III-V MOSFETs significantly increases, as shown in Fig. 5. In particular, heavily-doped III-V MOSFETs can provide about 1.5 times the current drivability of Si-based MOSFETs even at the ballistic limit.

IV. Conclusion

For III-V MOSFETs to definitely outperform Si and Ge MOSFETs under quasi-ballistic transport, a high source and drain doping concentration is required because the parasitic resistance in drain and source starvation impede the high mobility materials providing a higher current drive. Our Monte Carlo simulation showed that if a heavily-doped source and drain can be achieved, III-V MOSFETs can provide at least 1.5 times the current drivability of Si-based MOSFETs even for the channel lengths of several tens of nanometers.

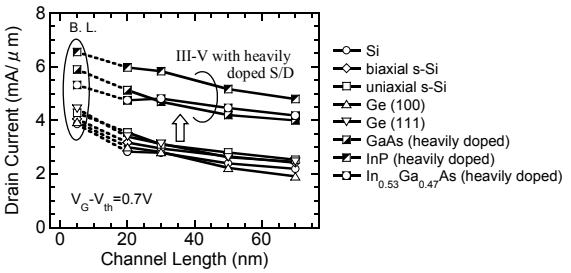

Fig. 5. Drive current enhancement due to heavily-doped S/D in III-V MOSFETs. V_G-V_{th} = 0.7 V and V_D = 0.5 V.

References

[1] S. Takagi, T. Irisawa, T. Tezuka, T. Numata, S. Nakaharai, N. Hirashita, Y. Moriyama, K. Usuda, E. Toyoda, S. Dissanayake, M. Shichijo, R. Nakane, S. Sugahara, M. Takenaka, and N. Sugiyama, "Carrier-transport-enhanced channel CMOS for improved power consumption and performance," *IEEE Trans. Electron Devices*, vol. 55, no. 1, pp. 21-39, Jan. 2008.

[2] T. Mori, Y. Azuma, H. Tsuchiya, and T. Miyoshi, "Comparative study on drive current of III-V semiconductor, Ge and Si channel n-MOSFETs based on quantum-corrected Monte Carlo simulation," *IEEE Trans. Nanotechnology*, vol. 7, no. 2, pp. 237-241, Mar. 2008.

[3] Y. Azuma, T. Mori, and H. Tsuchiya "Drive current of ultrathin Ge-on-insulator n-channel MOSFETs," *Phys. Stat. Sol. (c)*, vol. 5, no. 9, pp. 3153-3155, Mar. 2008.

[4] K. Uchida, T. Krishnamohan, K. C. Saraswat, and Y. Nishi, "Physical mechanisms of electron mobility enhancement in uniaxial stressed MOSFETs and impact of uniaxial stress engineering in ballistic regime," in *IEDM Tech. Dig.*, 2005, pp. 135-138.

[5] T. Maegawa, T. Yamauchi, T. Hara, H. Tsuchiya, and M. Ogawa, "Strain effects on electronic bandstructures in nanoscaled silicon: From bulk to nanowire," *IEEE Trans. Electron Devices*, vol. 56, no. 4, pp. 553-559, Apr. 2009.

[6] M. V. Fischetti, S. Jin, T.-W. Tang, P. Asbeck, Y. Taur, S. E. Laux, M. Rodwell, and N. Sano, "Scaling MOSFETs to 10nm: Coulomb effects, source starvation, and virtual source model," *J. Comp. Electron*., vol. 8, no. 2, pp. 60-77, Jun. 2009.

[7] H. Tsuchiya, M. Horino, M. Ogawa, and T. Miyoshi, "Quantum transport simulation of ultrathin and ultrashort silicon-on-insulator metal-oxide-semiconductor field-effect transistors," *Jpn. J. Appl. Phys.*, vol. 42, no. 12, pp. 7238-7243, Dec. 2003.

[8] M. V. Fischetti and S. E. Laux, "Monte Carlo simulation of transport in technologically significant semiconductors of the diamond and zinc-blende structure–Part II: Submicrometer MOSFET's," *IEEE Trans. Electron Devices*, vol. 38, no. 3, pp. 650-660, Mar. 1991.

[9] T. Kanazawa, H. Saito, K. Wakabayashi, T. Tajima, R. Terao, Y. Miyamoto, and K. Furuya, "Fabrication of InP/InGaAs undoped channel MOSFET with selectively regrown N^+-InGaAs source region," in *SSDM Ext. Abst.*, 2009, pp. 246-247.

[10] M. V. Fischetti, L. Wang, B. Yu, C. Sachs, P. M. Asbeck, Y. Taur, and M. Rodwell, "Simulation of electron transport in high-mobility MOSFETs: Density of states bottleneck and source starvation," in *IEDM Tech. Dig.*, 2007, pp. 109-112.

[11] S. E. Laux, "A simulation study of the switching times of 22- and 17-nm gate-length SOI nFETs on high mobility substrates and Si," *IEEE Trans. Electron Devices*, vol. 54, no. 9, pp. 2304-2320, Sep. 2007.

[12] H. Tsuchiya, K. Fujii, T. Mori, and T. Miyoshi, "A quantum-corrected Monte Carlo study on quasi-ballistic transport in nanoscale MOSFETs," *IEEE Trans. Electron Devices*, vol. 53, no. 12, pp. 2965-2971, Dec. 2006.

[13] M. J. Antonell, C. R. Abernathy, V. Krishnamoorthy, R. W. Gedridge, Jr., and T. E. Haynes, "Thermal stability of heavily tellurium-doped InP grown by metalorganic molecular beam epitaxy," *J. Electron. Materials*, vol. 26, no. 11, pp. 1283-1286, 1997.

[14] H. Q. Zheng, K. Radahakrishnan, S. F. Yoon, and G. I. Ng, "Electrical and optical properties of Si-doped InP grown by solid source molecular beam epitaxy using a valved phosphorus cracker cell," *J. Appl. Phys.*, vol. 87, no. 11, pp. 7988-7993, Jun. 2000.